Materials Science-Poland, 32(2), 2014, pp. 281-291
http://www.materialsscience.pwr.wroc.pl/
DOI: 10.2478/s13536-013-0173-x

VERSITA

Parametric optimization of $NiFe_2O_4$ nanoparticles synthesized by mechanical alloying

A. HAJALILOU[1]*, M. HASHIM[1], R. EBRAHIMI-KAHRIZSANGI[2], H. MOHAMED KAMARI[3], S. KANAGESAN[1]

[1]Material Synthesis and Characterization Laboratory, Institute of Advanced Nano Technology (ITMA), Universiti Putra Malaysia, 43400 UPM Serdang, Selangor, Malaysia

[2]Materials Engineering Department, Islamic Azad University, Najafabad Branch, Isfahan, Iran

[3]Physics Department, Universiti Putra Malaysia, 43400 UPM Serdang, Selangor, Malaysia

In this study, the Taguchi robust design method is used for optimizing ball milling parameters including milling time, rotation speed and ball to powder weight ratio in the planetary ball milling of nanostructured nickel ferrite powder. In fact, the current work deals with $NiFe_2O_4$ nanoparticles mechanochemically synthesized from NiO and Fe_2O_3 powders. The Taguchi robust design technique of system optimization with the L9 orthogonal array is performed to verify the best experimental levels and contribution percentages (% ρ) of each parameter. Particle size measurement using SEM gives the average particle size value in the range of 59 – 67 nm. X-ray diffraction using Cu Kα radiation is also carried out to identify the formation of $NiFe_2O_4$ single phase. The XRD results suggest that $NiFe_2O_4$ with a crystallite size of about 12 nm is present in 30 h activated specimens. Furthermore, based on the results of the Taguchi approach the greatest effect on particle size (42.10 %) is found to be due to rotation speed followed by milling time (37.08 %) while ball to powder weight ratio exhibits the least influence.

Keywords: *magnetic materials; microstructure; X-ray diffraction; crystal structure*

1. Introduction

Recently, synthesis of nanosized $NiFe_2O_4$ powder particles has attracted the attention of researchers due to their high saturation magnitization, low eddy current loss in alternating applications, and high magnetocrystalline anisotropy. Soft ferromagnetic $NiFe_2O_4$ is one of the most important ferrites of the inverse spinel family which is widely used in magnetic information storage instruments, sensors, drug delivery agents, catalysis, etc. [1–5]. By decreasing the particle size of this ferrite to about 10 nm, significant changes may occur in its physical, magnetic, and microstructural properties that include the anomalous cation ratio at the octahedral and tetrahedral sites in small particles, increased external field, effective anisotropy constant [6], and surface spin disorder [7]. Thus, evaluation of ferrite structure and crystallite size is essential for selecting the proper method of synthesizing $NiFe_2O_4$ nanoparticles. Different methods have been used so far to fabricate $NiFe_2O_4$ nanoparticles such as sol-gel [8], chemical route [9], hydrothermal [10], co-precipitation [11] and ball milling method [12]. In this study, mechanical alloying was chosen for synthesizing $NiFe_2O_4$ nanoparticles. In this method, the magnetic properties and final structure of the product may be affected by the different process parameters such as type of mill, milling speed, milling container, and ball to powder ratio [13]. Previous studies have simulated the dynamics effects of the milling process based on the rate of collision, ball velocity, and kinetic energy between powder particles during mechanical activation [14–17]. A number of relations have been suggested [16, 17] for calculating the impact of velocity and the kinetic energy transferred from balls to powder particles. These relations have been em-

*E-mail: e.hajalilou@yahoo.com

ployed in the present study based on the following equations:

$$||\vec{V}_c||^2 = (R\Omega)^2 + (r - r_b)^2\omega^2\left(1 + \frac{2\omega}{\Omega}\right) \quad (1)$$

$$E_k = \frac{1}{2}m||\vec{V}_c||^2 \quad (2)$$

where, r, R, m, Ω, ω, and r_b represent the vial radius, the distance between the vial center and disc center, the mass of balls, the speed of disc rotation, the speed of vial rotation, and the radius of the balls, respectively.

The Taguchi robust design method provides an efficient, simple and systematic approach for verifying the optimal factors involved in the production process. Moreover, it is used to examine all factors with only a small number of tests. A statistical analysis of variance (ANOVA) can also be executed to determine the statistically significant factors. Thus, the optimal parameters can be anticipated by the orthogonal array experiments [18, 19]. In this study, the main factors of the planetary ball milling (i.e., milling time, rotation speed, and ball to powder weight ratio) were optimized using this technique.

The contents of each phase produced in the as-synthesized product were determined using the integrated X-ray diffraction peak intensities based on the following equation:

$$W_x = \frac{A_x^{(hkl)}}{\sum xA_x^{(hkl)}} \quad (3)$$

where, W_x and A_x, designate the calculated fraction for one compound and the integrated diffraction intensity of the major peak of compound X, respectively.

2. Experimental

Commercial nickel and iron oxide powders were purchased from Alfa Aesar and used as starting materials. To produce the $NiFe_2O_4$, the powders of NiO and Fe_2O_3 were mixed in a stoichiometric ratio of 1:1 (molar mass). The mechanical activation process was performed in a high energy planetary ball milling machine. The characteristics of the milling tool and the experimental conditions are described below:

Vail (stainless steel, volume 150 ml), ball (stainless steel, 5 balls 18 mm in diameter), ball to powder ratio (10:1, 20:1, and 30:1), atmosphere (argon), milling time (0, 4, 6, 10, 12, 14, 18, 24 and 30 h). The terms r, R, and Ω as defined above were R = 120 mm, r = 45 mm, and $150 < \Omega < 600$ rpm.

The X-ray diffraction spectrometer (XRD) was used to analyze phase changes during the ball milling process. The Bragg diffraction angle (2θ) in all the experiments was chosen in the range of 20 – 80 degrees, applying the Cu Kα of $\lambda = 0.154$ nm.

Since the crystallite size and lattice strain are the most important factors that can influence such properties as microstructure and magnetic properties, it was decided to apply the modified Scherrer equation [20] to report the precise crystallite size and lattice strain. Scherrer equation (i.e., $d = K\lambda/\beta\cos\theta$) was first developed in 1918 to compute crystallite size (d) using an X-ray diffraction radiation wavelength (λ) by considering full width at half maximum peak (β) at the Bragg diffraction angle (2θ). In this equation, K is the shape factor whose value can vary from 0.62 to 2.08, but a value of about 0.9 is commonly chosen for this parameter. Evidently, this equation will only yield a mean crystallite size and will not provide information on particle size distribution or the scope of grain agglomeration.

The first point to note about this equation is that it cannot be used to calculate lattice strain. Moreover, if all the peaks on the diffraction pattern have the same value as d, then $\beta\cos\theta$ must also have the same value. This signifies that for a crystallite size (d) of 5 nm and $\lambda = 0.154$ nm, for instance, the peak at Bragg diffraction angle (2θ) of 10° must be ten times narrower than the peak at $2\theta = 70°$; this situation is never observed. Hence, Monshi [21] modified this equation as $\text{Ln}\beta = \text{Ln}(k\lambda/d) + \text{Ln}(1/\cos\theta)$ by using the least squares method to minimize the errors induced. The $\text{Ln}\beta$ plots the inverse of $\text{Ln}(1/\cos\theta)$ to obtain the intercepts of a least square line regression.

The Scanning Electron Microscopy (SEM) using a FEINOVA nano SEM 230 machine was used to observe both the topography and morphology of the particles and to measure their grain size and distribution.

3. Results and discussion

3.1. Evaluation of the effect of milling time on crystallite size

Duration of mechanical alloying is one of the fundamental parameters usually exploited to achieve a steady-state (SS) between the breaking and rewelding (cold working) of powder particles. The different parameters of milling type, ball to powder weight ratio and rotation speed can vary the combustion reaction time during the ball milling process. In fact, to achieve the optimum milling time, the above parameters should be adjusted in relation to each other depending on the system selected. Fig. 1 shows the X-ray diffraction patterns of the samples after different milling times while ball to powder weight ratio (BPR) is kept constant at 20:1 and the vial's rotation speed at 600 rpm. The spectra of NiO and Fe_2O_3 are visible in this XRD pattern in the initial powder after the simple mixing. The major peaks of the two initial raw materials, i.e. NiO at $2\theta = 43.298$ and Fe_2O_3 at $2\theta = 33.155$, can be accordingly indexed to ICCD cards of 044-115 for NiO and 01-079-1741 for Fe_2O_3. The phase changes occurring after different milling times confirm the effect of milling time on powder particles. The peaks of nickel ferrite appeared in the XRD pattern after increasing the milling time by up to 18 h. Further increase of milling time to 30 h, caused nickel ferrite to become almost amorphous due to the transfer of high energy to powder particles.

The refinement of mean particle size during a milling process can be stated with this relationship applying a simple model for the refinement of nanocrystalline particle size [13]:

$$D = Kt^{-\frac{2}{3}} \tag{4}$$

where t is the milling time, D is the particle size and K is the constant. However, since a number of process variables as mentioned by Suryanarayana [13] earlier, could influence the particle size achieved, more systematic experiments are needed before solid explanations can be made.

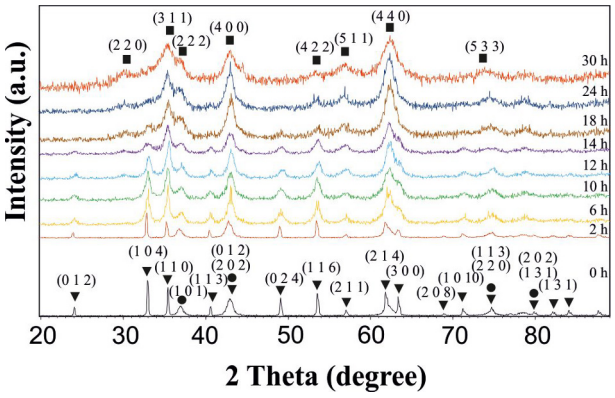

Fig. 1. X-ray diffraction patterns taken from the NiO/Fe_2O_3 powder mixture after different milling times by keeping constant RPM (600 rpm) and BPR (20:1); NiO (●), Fe_2O_3 (▼), $NiFe_2O_4$ (■).

Fig. 2 displays SEM images of $NiFe_2O_4$ ferrite after being milled for 18 and 30 h. After 18 h milling, the size ranges from about 48 nm to 89 nm with a mean particle size of about 59 nm. After further milling up to 30 h, the powders exhibit high agglomeration of particles as can be seen in the SEM image. This is due to the high energy transferred to the powder particles after 30 h of milling. The size ranges from about 57 to 101 nm with a mean particle size of about 67 nm.

The internal lattice strain and average crystallite size of the ball-milled samples as a function of milling time is illustrated in Fig. 3. A gradual decrease is observed in average crystallite size from 33 (2 h milling) to approximately 12 nm (24 h milling) followed by a slight increase in crystallite size of about 1.9 percent (about 13 nm) after 30 h of milling. To explain this phenomenon, one can consider the fact that the ball milling process leads to the refinement of crystallite size by breaking and rewelding of powder particles, but that after a certain (critical) milling time, the powder particles stick together and become agglomerated due to an abrupt increase in temperature inside the vial. Regarding lattice strain, the effect of

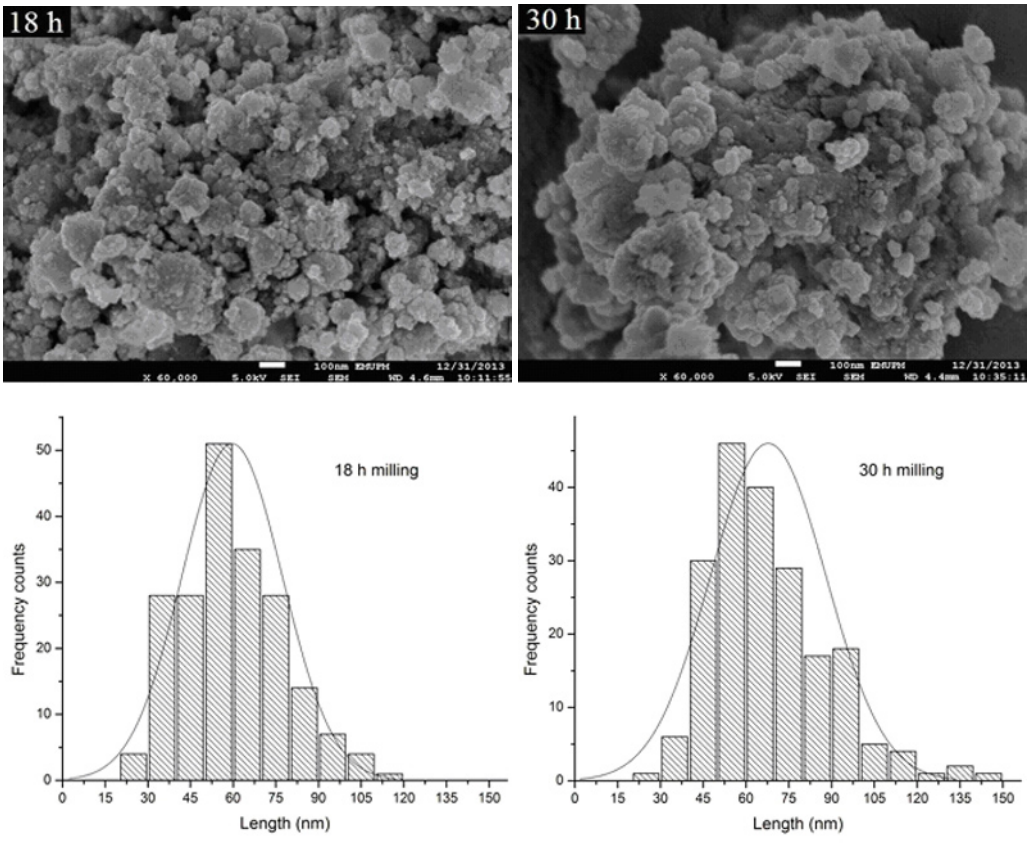

Fig. 2. SEM images of $NiFe_2O_4$ nanoparticles after 18 and 30 h milling.

crystallite size due to increased milling time has been the subject of controversy. Increased value of lattice strain is associated with the creation of lattice imperfections such as grain boundaries, dislocations, etc. These defects provide the short-circuit path to diffusion at low temperatures and result in the production of a large number of defects. After a certain milling time (24 h) passed, the sudden increase in temperature led to grain growth and resulted in an easier diffusion process in the lattice than at grain boundaries and other high energy sites. Lattice strain, therefore, decreased after 24 h of milling.

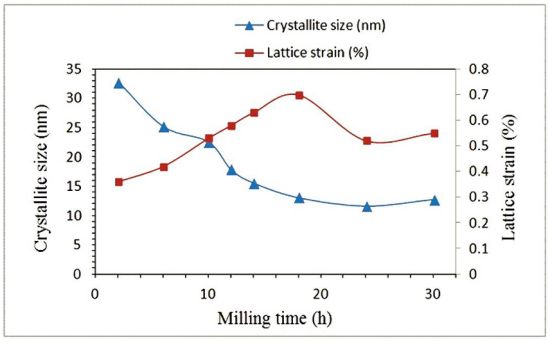

Fig. 3. The internal lattice strain and average crystallite size as a function of milling time.

As it was the aim of this study to investigate the effects of milling time on the properties of powder particles, the same unchanging conditions were initially employed during the milling from 0 to 30 hours. In other words, BPR was taken constant at 20:1 and the rotation speeds of the vial and the disc were fixed at 600 and 400 rpm, respectively. The characteristics of the powder particles influenced by various milling times are given in Table 1. As can be seen, increasing milling time led to increased collision velocity and kinetic energy but to decreasing crystallite size.

Table 1. Structural properties of powder particles as a function of milling time.

Milling time (h)	Proportion of ω(rpm)/Ω(rpm)	Collision velocity, V_c (m/s)	Kinetic energy per hit (J)	Crystallite size (nm)	Lattice strain (%)	Wt. (%) $NiFe_2O_4$
2	600/400	0.2848	0.2097	32.8	0.36	–
6	600/400	0.3653	0.3732	25.2	0.42	–
10	600/400	0.4562	0.5832	22.6	0.53	–
12	600/400	0.5475	0.8397	17.9	0.58	–
14	600/400	0.6337	1.1435	15.6	0.63	–
18	600/400	0.7307	1.4938	13.1	0.71	80
24	600/400	0.7506	1.5436	11.6	0.52	100
30	600/400	0.9214	2.3334	12.2	0.55	100

3.2. Evaluation of the effect of rotation speed on the crystallite size

A similar effect on crystallite size was observed by changing rotation speed and fixing milling time to 30 h and BPR at 20:1. Increasing rotation speed caused powder particle size to decrease and lattice strain to increase. The X-ray diffraction patterns of ball milled samples at different rotation speeds are shown in Fig. 4.

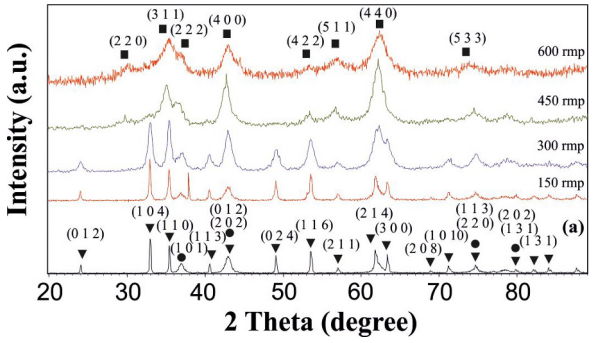

Fig. 4. XRD patterns of NiO/Fe_2O_3 powders ball milled at different RPMs by keeping constant milling time at 30 h and BPR 20:1; NiO (●), Fe_2O_3 (▼), $NiFe_2O_4$ (■).

As can be observed, when mechanical activation was run at 150 rpm, no significant modification was observed in the relevant XRD pattern peaks compared with those for the simple mixing of initial powders. However, the broadening of the crystallite peaks was observed which can be related to the refinement of crystallite size and the increment of internal lattice strain. By increasing the rotation speed to 300 rpm, the peak position of the Fe_2O_3 phase slightly shifted toward higher Bragg diffraction angles and the intensity of the peaks decreased. For instance, the three major peaks of Fe_2O_3 moved to the Bragg diffraction angle positions of 33.470, 35.853, and 54.205 when compared with the reference peak positions. It is noteworthy that by increasing rotation speed above 450 rpm, the position of the peaks shifted to lower Bragg diffraction angles as compared to the situation when the rotation speeds were 300 or 450 rpm. This could be associated with the solid solution formation of (Fe, Ni) O with FCC structure. The value of the $NiFe_2O_4$ phase increased from 68.2 wt.% at a rotation speed of 450 rpm and a transferred energy of 1.5335 J/hit to 92.4 wt.% at a rotation speed of 600 rpm and a transferred energy of 2.3334 J/hit. This increase in the percentage of the $NiFe_2O_4$ phase with the rising energy transferred to the powder is due to the effective diffusion of atoms at higher rotation speeds. As shown in Table 2, more energy is imparted to powder particles by elevating the rotation speed, which results in the development of crystal defects such as dislocations, vacancy, and grain boundaries. In addition, the refinement of crystallite size leads to short-circuit diffusion and the existence of crystal defects results in increased solubility of elements in the crystal lattice. Therefore, facilitating the diffusion mechanism leads to an increase in the amount of the $NiFe_2O_4$ phase through increased rotation speed [22]. Since crystallite size and lattice strain are the factors that affect peak broadening, we calculated their values using the

modified Debye-Scherrer equation as reported in Table 2.

Moreover, lattice parameter is an important factor which can be associated with the displacement of position peaks. Therefore, the lattice parameter of $NiFe_2O_4$ was computed using the following equation [23]:

$$a = d_{(hkl)}\sqrt{h^2 + k^2 + l^2} \tag{5}$$

The values for the lattice parameter of nickel ferrite were calculated as 0.8278 and 0.8248 nm for 450 and 600 rpm, respectively. This indicates that the lattice parameter depends on rotation speed in such way that increasing the rotation speed decreases its value. In addition, the values of lattice parameter obtained for the $NiFe_2O_4$ single phase produced at 450 and 600 rpm were less than those reported for the bulk value of $NiFe_2O_4$ (a = 0.8339 nm) [24]. This is due to the reduction of powder particles as well as the accumulation of defects as a result of frequent breaking and rewelding of powder particles at high rotation speeds during the ball milling process.

3.3. Evaluation of the effect of ball to powder weight ratio (BPR) on crystallite size

As already mentioned, ball milling is a complicated process that requires the optimization of a number of variable parameters in order to obtain products with desirable magnetic properties. The effects of varying values of BPR on particle size for a milling time of 30 h and a constant rotation speed of 600 rpm are shown in Fig. 5. As can be observed, the single phase of nickel ferrite was produced for all the ball to powder weight ratios of 10:1, 20:1, and 30:1. The only significant discrepancy can be related to the varying powder particle sizes which were found to be 14.3, 12.2, and 16 nm at 10:1, 20:1, and 30:1 BPRs, respectively. In fact, by increasing the ratio of ball to powder weight, the amount of powder charged inside the vial decreases, leaving more space inside the vial which allows the velocity of ball-powder collisions to increase and much more energy to be transferred to powder particles. When the value of BPR was raised to 30:1, contrary to our expectation, the powder particle size was seen to increase, indicating that when the amount of powder decreases, the greater amount of energy transferred to powders leads to increase heat inside the vial which finally causes the agglomeration of powder particles.

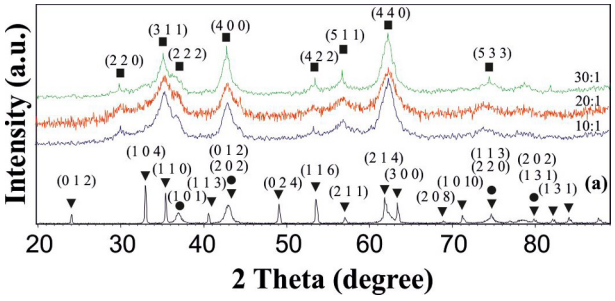

Fig. 5. XRD pattern of $NiFe_2O_4$, 30 h milling as a function of BPR (by keeping constant milling time at 30 h and RPM at 20:1); NiO (●), Fe_2O_3 (▼), $NiFe_2O_4$ (■).

4. Taguchi method

The Taguchi robust experimental design method was introduced in 1960 by Professor Taguchi. This method not only minimizes the number of experiments to determine the optimal conditions but also dramatically saves time and money for the tests required [25]. According to this method, selected parameters and levels of several orthogonal arrays are used as the matrix experiments. In this way, the changes caused by the introduction of each takes the signal to noise ratio as the experimental conditions. The highest signal-to-noise ratio is chosen as the optimal condition [26]. In this study, the Taguchi method briefly described below was used to determine the optimum conditions and the effects of synthesis parameters on the particle size of nickel ferrite.

1. The signal factor (S) and noise factor (N) accompanied by the relevant level are selected. In fact, signal factors are input parameters which can be changed in order to achieve optimal conditions in laboratory experiments in terms of selected levels and matrix of experiments. Noise factor refers to all the factors that cause changes in the

Table 2. Structural properties of powder particles as a function of rotation speed.

Milling time (h)	Proportion of ω(rpm)/Ω(rpm)	Collision velocity, V_c (m/s)	Kinetic energy per hit (J)	Crystallite size (nm)	Lattice strain (%)	Wt. (%) of $NiFe_2O_4$
30	150/92	0.1868	0.1231	45.6	0.471	–
30	300/183	0.1990	0.1971	22.3	0.531	–
30	450/274	0.8287	1.8821	15.2	0.651	92
30	600/364	0.9214	2.3334	12.2	0.550	100

conditions and are assumed to be constant during the experiment.

2. The loss functions are calculated to determine modifications between the experimental results and optimal values. Depending on the circumstances, this function is calculated using the following equations:
   First state: The smallest amount of reagent is optimal:

$$SB = \frac{1}{2}\sum yi^2 \tag{6}$$

   Second state: The amount is greater than the optimum reagent:

$$LB = \frac{1}{n}\sum \frac{1}{yi^2} \tag{7}$$

   Third state: The nominal size is optimal:

$$NB = \frac{1}{2}\sum (y_i - y_0)^2 \tag{8}$$

   where, n is the number of experiment repeatability, y_i is the measured output, and y_0 is the optimal nominal size.
3. The total value of signal-to-noise can be calculated for each parameter based on the following equation:

$$S/N = -10\log\left[\frac{1}{n}\sum_{i=1}^{ni}\frac{1}{yi^2}\right] \tag{9}$$

4. The signal to noise ratio is calculated for each level of the parameters.
   In the Taguchi method, parameters with the highest signal-to-noise ratio (regardless of the type of loss function) are introduced as optimal levels.
5. The significance of each parameter is determined using ANOVA.
6. Data is analyzed and the optimum output is predicted.
7. Validation and verification tests are performed to confirm the results.

4.1. Experiment design

4.1.1. Controlling and non-controlling factors

Milling time, rotation speed, and ball to powder weight ratio (BPR) as parameters dependent on crystallite size were selected as the signal factors. However, the molar ratio could also be chosen as a noise factor as it was constant during the trials. The orthogonal array 9 (L9) was performed to optimize the three variable parameters of the mechanical alloying process. Table 3 lists the variables and their levels for each parameter. To increase the accuracy, each experiment was repeated three times and the equal mass was selected and measured after mixing the crystals.

Table 3. The main controlling parameters and their levels.

Factors	Levels		
	1	2	3
Milling time (h)	6	18	30
Ball to powder ratio (BPR)	10:1	20:1	30:1
Rotation speed (rpm)	150	400	600

4.1.2. Determining the optimal conditions

For this purpose, the X-ray diffraction pattern obtained from laboratory experiments was used

to calculate the crystallite size using the Scherrer equation:

$$d = 0.9\lambda/\beta\cos\theta \tag{10}$$

where, d is the average crystallite size, θ is the Bragg's diffraction angle, and β is the full width at half maximum (FWHM).

The FWHM was adjusted as β, which can be related to the discrepancy in the integral profile width between a measured FWHM (βi) and equipment peak broadening (βe); therefore, the refinement β was used based on the following equation to remove the errors due to the instruments [27]:

$$\beta^2 = \beta i^2 - \beta e^2 \tag{11}$$

Prior to estimating the crystallite size and lattice strain from the XRD peaks, the background was automatically eliminated to refine the data and the exact positions of kα1 and kα2 radiation were analyzed using the X-Pert High Score software:

$$\frac{k\alpha 2}{k\alpha 1} = 0.51 \tag{12}$$

X-Pert High Score software executes the Pseudo-Voigt profile which is the weighted average between a Gaussian and a Lorentz function:

$$G_{ik} = \gamma\frac{C_0^{\frac{1}{2}}}{H_k\pi}[1 + C0X_{ik}^2]^{-1} + (1-\gamma)\frac{C_1^{\frac{1}{2}}}{H_k\pi^{\frac{1}{2}}}\exp\left[C1X_{ik}^2\right] \tag{13}$$

where, C_0 and C_1 are taken to be 4 and $4 \times \ln 2$, respectively; H_k is the β of the K_{th} Bragg reflection; and X_{ik} is equal to $(2\theta i - 2\theta k)/H_k \cdot \gamma$ is a variable "mixing" parameter given on account of the amount of Lorentzian profile versus the amount of Gaussian profile, which ultimately provides the overall profile shape.

Table 4 displays the orthogonal array used and the calculated crystallite size for each stage, accompanied by its S/N ratio in each experiment. The average S/N ratios for each level of the parameters in terms of the crystallite size are presented in Table 5 and in Fig. 6. Based on the following equation used for calculating the value of R, one rank is assigned to each variable. The largest value of R is the effective factor. In addition, the highest value of S/N for each variable represents the optimal experimental conditions [28]:

$$R = \left(\text{high}\frac{S}{N} - \text{low}\frac{S}{N}\right) \tag{14}$$

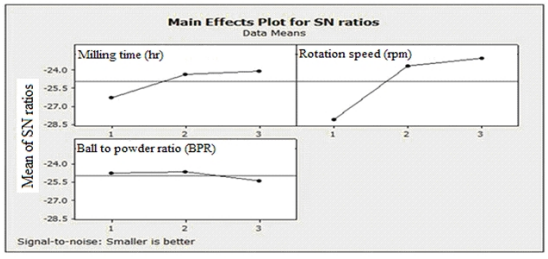

Fig. 6. Mean S/N ratio for each level of the parameters for crystallite size based on Taguchi design.

As can be seen, the maximum value of R was obtained for the rotation speed. The highest values are seen to have the greatest effect on the final outcome while the lowest have the least impact, indicating that rotation speed has the highest effect on particle size during the ball milling process.

The average crystallite size for each level of parameters based on Taguchi design is shown in Fig. 7. Comparison of rotation speed and the two other parameters for the greatest change in crystallite size between levels 1 and 2 indicates that rotation speed has a significant effect on crystallite size during the ball milling process.

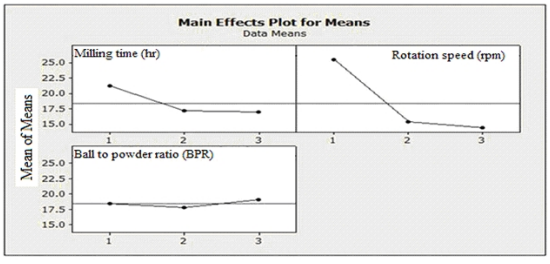

Fig. 7. Average crystallite size for each level of the parameters based on Taguchi design.

The predicted values of Taguchi design independently for S/N ratio and mean crystallite size

Table 4. The conditions of the experiments based on the orthogonal array L9.

Experiment	Milling time (h)	BPR	Rotation speed (rpm)	crystallite size (nm)	dB (S/N ratio)	Taguchi predicted S/N ratio	Taguchi predicted crystallite size (nm)
1	1	1	1	28.3	−29.0357	−28.0058	24.8556
2	1	2	2	17.5	−24.8608		
3	1	3	3	17.8	−25.0084		
4	2	1	2	23.6	−27.4582		
5	2	2	3	14.7	−23.3463		
6	2	3	1	13.2	−22.4115		
7	3	1	3	24.6	−27.8187		
8	3	2	1	13.9	−22.8603		
9	3	3	2	12.2	−21.7272		

Table 5. The mean S/N ratio for each level of the parameters for crystallite size based on Taguchi design.

Parameter	Level			Rank
	1	2	3	
Milling time (h)	−26.30	−24.41	−24.14	2
Rotation speed (rpm)	−28.10	−23.69	−23.05	1
Ball to powder weight ratio	−24.77	−24.68	−25.39	3

for each parameter are presented in Table 6. Based on these results, it may be concluded that the optimum conditions for the synthesis of nickel ferrite nanoparticles can be achieved by ball milling for 18 h at a rotation speed of 600 rpm and with a ball to powder weight ratio of 20:1.

Table 6. The predicted values of Taguchi design for S/N ratio and mean crystallite size for each parameter.

Parameter	S/N ratio	Mean
Milling time (h)	−24.4054	17.1667
BPR	−28.1042	15.35
Rotation speed (rpm)	−25.3911	19.0333

5. Analysis of variance (ANOVA)

The analysis of variance (ANOVA) was performed to examine the relative effect of each parameter on crystallite size and to find out which process parameter had a significant effect on the output results. For this purpose, the total variability of the S/N ratios was determined as calculated by subtracting the sum of square deviations (SS) based on the data reported earlier in Table 5 from the total mean of the S/N ratio (S_m). The following equations were used for the ANOVA analysis for each parameter [29]:

$$SS_i = \left[\frac{jmi_1}{j_1} + \frac{jmi_2}{j_2} + \ldots\right] - S_m \qquad (15)$$

$$S_m = \frac{\left(\sum_{i=1}^{i=n} \frac{S}{Ni}\right)^2}{n} \qquad (16)$$

where, SS_i is the sum of the squares for each parameter; j is the number of each parameter in the orthogonal array; mi_1 and mi_2 are the means of S/N ratios for the related level and the factor i.

MS_i (mean of the sum of squares for each parameter), S_t (total sum of squares) and MS_e (error

of the sum of squares) can be computed from the following equations, respectively:

$$MS_i = \frac{SS_i}{DF\text{ofi}} \tag{17}$$

$$S_t = \sum_{i=1}^{i=n} \left(\frac{S}{Ni}\right)^2 - S_m \tag{18}$$

$$MS_e = S_T - \sum SS_i \tag{19}$$

The values for the relative distribution of each parameter were obtained from:

$$MS_i = \frac{SS_i}{DF_i} \tag{20}$$

$$F_i = \frac{MS_i}{MS_e} \tag{21}$$

where, DF_i is the degree of freedom which was obtained from the number of experiments minus one. In fact, the degree of freedom for each parameter is equal to the number of levels of that parameter minus one.

Percent of contribution for parameter i can be calculated from the equation below:

$$\rho\ (\%) = \frac{SS_i - DF_i(MS_e)}{S_T} \times 100 \tag{22}$$

The results of the calculated factors are presented in Table 7. The results suggest that the rotation speed has the greatest influence on crystallite size with a contribution of 42.10 % while the milling time is the second most important parameter with a contribution of 37.08 %. The ball to powder weight ratio of 20.82 % has the least effect on crystallite size.

Table 7. ANOVA for S/N ratio of the crystallite size.

Parameter	DF	SS	MS	ρ (%)
Milling time (h)	2	9.79	4.89	37.08
BPR	2	5.54	2.77	20.82
Rotation speed (rpm)	2	11.11	5.55	42.10
Total	8	26.44	–	100

6. Conclusion

The nanosized nickel ferrite powder particles were successfully produced by the mechanical activation process. The results showed that ball milling up to 18 h resulted in the reaction of the NiO/Fe_2O_3 in the combustion mode producing the single phase of $NiFe_2O_4$ nanostructure. Meanwhile, different parameters associated with the mechanical activation technique were investigated using the Taguchi robust design method. As the three parameters of milling time (h), ball to powder weight ratio and rotation speed were used in the study of the process, the orthogonal array nine (L9) was performed to optimize the experimental conditions in order to achieve the least crystallite size. Regarding the fact that the crystallite size of the nickel ferrite after 30 h of milling was obtained to be about 12 nm, the Taguchi design indicated that the rotation speed (rpm) with a contribution of 42 % had the greatest influence on crystallite size during the mechanical activation process. Under the optimized conditions obtained from this method, nickel ferrite nanoparticles (in the range of 12 – 17 nm in size) with a narrow particle size distribution were prepared. The results obtained are consistent with the data obtained from the analysis by the Taguchi method. In conclusion, it was found that the ball milling process has potential capability for the large scale fabrication of nanosized powder particles at low costs.

References

[1] ZHANG J., SHI J., GONG M., *J. Solid State Chem.*, 182 (8) (2009), 2135.
[2] SAFARIK I., SAFARIKOVA M., *Nanostruct. Mater.*, Springer, Vienna, (2002), 1.
[3] PILENI M.P., *Nat. Mater.*, 2 (2003), 145.
[4] SUN J., ZHOU S., HOU P., YANG Y., WENG J., LI X., LI M., *J. Biomed. Mater. Res. A*, 80A (2007), 333.
[5] SALAVATI-NIASARI M., DAVAR F., MAHMOUDI T., *Polyhedron*, 28 (2009), 1455.
[6] MATHEW D.S., JUANG R.S., *Chem. Eng. J.*, 129 (2007), 51.
[7] KODAMA R.H., BERKOWITZ A.E., MCNIFF E., FONER J., FONER S., *Phys. Rev. Lett.*, 77 (1996), 394.
[8] SRIVASTAVA M., OJHA A.K., CHAUBEY S., MATERNY A., *J. Alloy. Compd.*, 481 (2009), 515.
[9] MAENSIRI S., MASINGBOON C., BOONCHOM B., SUPAPAN S., *Scripta Mater.*, 56 (2007), 797.

[10] XU Q., WEI Y., LIU Y., JI X., YANG L., GU M., *Solid State Sci.*, 11 (2009) 472.
[11] ARULMURUGAN R., VAIDYANATHAN G., SENDHILNATHAN S., JEYADEVAN B., *J. Magn. Magn. Mater.*, 298 (2006), 83.
[12] MUTHUSELVAM I.P., BHOWMIK R.N., *Solid State Sci.*, 11 (2009), 719.
[13] SURYANARAYANA C., *Prog. Mater. Sci.+*, 46 (2001), 1.
[14] MAURICE D.R., COURTNEY T.H., *Metall. Mater. Trans. A*, 21 (1990), 289.
[15] MAURICE D.R., COURTNEY T.H., *Metall. Mater. Trans. A*, 26 (1995), 2431.
[16] COOK T.M., COURTNEY T.H., *Metall. Mater. Trans. A*, 26 (1995), 2389.
[17] ABDELLAOUI M., GAFFET E., *J. Alloy. Compd.*, 209 (1994), 351.
[18] GARCIA-DIAZ A., PHILIPS D.T., *Principles of experimental design and analysis*, Chapman and Hall, London, 1995.
[19] MONTGOMERY D.C., *Design and analysis of experiments*, 4th ed., John Wiley and Sons, New York, 1997.
[20] KLUG H.P., ALEXANDER L.E., *X-ray Diffraction Procedures for Polycrystalline and Amorphous Materials*, 2nd ed., John Wiley and Sons, New York, 1974.
[21] MONSHI A., FOROUGHI M.R., MONSHI M.R., *World J. Nano Sci. Eng.*, 2 (2012), 154.
[22] GHEISARI KH., JAVADPOUR S., OH J.T., GHAFFARI M., *J. Alloy. Compd.*, 472 (2009), 416.
[23] CULLITY B.D., *Elements of X-ray Diffraction*, Addison Wesley Pub. Co. Inc., 1956, 42.
[24] QI W.H., WANG M.P., *Mater. Chem. Phys.*, 88 (2004), 280.
[25] ROY R.K., *A Primer on the Taguchi Method*, 2nd ed., Society of Manufacturing Engineers, 2010.
[26] ROSS P.J., TAGUCHI G., *Techniques for Quality Engineering*, McGraw-Hill, New York, 1988.
[27] PAIVA-SANTOS C.O., GOUVEIA H., LAS W.C., VARELA J.A., *Mater. Struct.*, 6 (1999), 111.
[28] ROSS P.J., *Taguchi Techniques for Quality Engineering*, 2nd ed., McGraw-Hill, Singapore, 1996.
[29] BENDELL A., DISNEY J., PRIDMORE W.A., *Taguchi Methods: Applications in World Industry*, IFS Publications, UK, 1989.

Received 2014-01-08
Accepted 2014-02-15